Original Article

Facile Biosynthesis of Gold Nanostructures Using Aqueous Extracts of *Scutellaria multicaulis* and *Heracleum persicum* Stems and *H. persicum* Fruits, and their Cytotoxicity Against Breast Cancer Cells

Zahra Gharari[1*], Hanie Sadeghinia[1], Parichehr Hanachi[1]

1. Department of Biotechnology, Faculty of Biological Sciences, Alzahra University, Tehran, Iran.

*** Corresponding Author:**
Zahra Gharari, PhD.
Address: Department of Biotechnology, Faculty of Biological Sciences, Alzahra University, Tehran, Iran.
Phone: +98 (914) 455 2393
E-mail: z.gharari@alzahra.ac.ir

Article info:
Received: 02 Jun 2025
Accepted: 03 Sep 2025

Keywords:
Anticancer, Antioxidant, Apoptosis, Gold nanoparticles (AuNPs), Green synthesis

ABSTRACT

Background: The introduction of highly specific drug nanoparticles (NPs) into cancer cells has demonstrated a broad therapeutic potential with diminished toxicity. Hence, the synthesis of nanoparticles has garnered significant interest among researchers

Objectives: This study presents an eco-friendly method for synthesizing gold NPs (AuNPs) using *Scutellaria multicaulis* and *Heracleum persicum* stem extracts, *Sanguisorba officinalis* root, and *H. persicum* fruit extracts, and evaluates their anticancer effects.

Methods: The characterization of AuNPs was studied using UV–visible, field emission scanning electron microscopy (FESEM), energy dispersive X-ray (EDX) spectroscopy, X-ray diffraction (XRD), dynamic light-scattering (DLS), Zeta potential (ZP), and Fourier-transform infrared spectroscopy (FTIR). Total phenolic content (TPC) and total flavonoid content (TFC) of AuNPs were evaluated using colorimetric analysis. MTT (3-(4,5-dimethylthiazol-2-yl)-2,5-diphenyltetrazolium bromide) and apoptosis assays were used to assay their cytotoxic potential.

Results: The absorption peaks were between 535 and 545 nm. FE-SEM and EDX analyses revealed that the AuNPs were oval in shape with a crystal size of 10-30 nm. XRD data showed the crystal structures of AuNPs to be 7.41, 7.61, 7.61, and 7.84 nm for stems of *S. multicaulis* (Sm-S)-AuNPs, stems of *H. persicum* (Hp-S)-AuNPs, roots of *S. officinalis* (So-R)-AuNPs, and fruits of *H. persicum* (Hp-F)-AuNPs, respectively. FT-IR suggested that elements such as phenolics, aromatic compounds, and proteins played a role in the reduction and stabilization of AuNPs. The mean size of AuNPs was ascertained using a Zetasizer, with measurements of 60.46, 41.2, 51, and 50.27 nm for Sm-S-AuNPs, Hp-S-AuNPs, So-R-AuNPs, and Hp-F-AuNPs, respectively. ZP analysis showed that AuNPs are negatively charged, indicating good dispersion stability. AuNPs had a high content of phenolic and flavonoid compounds

Citation Gharari Z, Sadeghinia H, Hanachi P. Facile Biosynthesis of Gold Nanostructures Using Aqueous Extracts of *Scutellaria multicaulis* and *Heracleum persicum* Stems and *H. persicum* Fruits, and their Cytotoxicity Against Breast Cancer Cells. Pharmaceutical and Biomedical Research. 2025; 11(4):311-330. http://dx.doi.org/10.32598/PBR.11.4.954.2

http://dx.doi.org/10.32598/PBR.11.4.954.2

and exhibited strong inhibitory effects on MDA-MB231 cell proliferation. Sm-S-AuNPs demonstrated anticancer effects in vitro by inducing oxidative stress and apoptosis.

Conclusion: Overall, the results affirm the potential of the examined plant extract as a viable raw biomaterial for the synthesis of biologically active AuNPs. These could be instrumental in developing novel antitumor agents to combat breast cancer.

Introduction

Presently, cancer research is shifting its focus towards identifying agents that contribute to a higher incidence of cancer. Simultaneously, the introduction of highly specific drug nanoparticles (NPs) into cancer cells has demonstrated a broad therapeutic potential with diminished toxicity. Hence, the synthesis of NPs has garnered significant interest among researchers [1]. Given the substantial challenges associated with the chemical and physical methods of nanoparticle production, it appears essential to employ cost-effective, safe, large-scale, and non-chemical methods.

Biomedical applications of gold NPs (AuNPs) have become a vibrant research area over the last few years [2]. An extensive range of potential biomedical applications has been investigated, encompassing protein and pathogen detection, drug and gene delivery [3], deoxyribonucleic acid (DNA) labeling, tissue engineering, fluorescent labeling, photothermal ablation, and use as contrast agents for magnetic resonance imaging (MRI) and other imaging techniques [4]. A significant portion of the research is focused on the biosynthesis, stabilization, and functionalization of AuNPs [5]. The most commonly reported stabilizing agents include transferrin, sodium citrate, and cetyltrimethylammonium bromide. Meanwhile, the species commonly used for functionalization include oligonucleotides, amines, antibodies, lipids, and peptides. AuNPs have attracted significant attention due to the simplicity of their production process, which enables precise control over their dimensions and shapes. Their optical properties and biocompatibility further enhance their appeal. But, it is crucial to note that repeated exposure can lead to a buildup of AuNPs in the body, potentially reaching harmful concentrations [6]. Consequently, most research on AuNPs is still in the experimental phase [7].

To improve the biocompatibility of AuNPs, the use of non-hazardous reagents is advised. The cornerstone of all AuNP-creation methods is the diminution of gold ions, usually in the guise of $HAuCl_4$ solutions. Numerous reducing agents have been recorded, with sodium borohydride and sodium citrate being the most common [8]. Additionally, the creation of AuNPs requires a safeguarding agent. This agent adheres to the surface of freshly biosynthesized NPs to curb further growth and prevent nanoparticle clustering. Consequently, by using suitable reduction and stirring techniques and selecting appropriate types of protective agents and their concentrations, the dimensions and shape of AuNPs can be controlled. Factors such as temperature, pH, agitation, and the application of external forces (e.g. ultrasound) are pivotal to the synthesis process. These elements have spurred numerous studies proposing novel methods for AuNP synthesis that employ environmentally friendly reduction agents and protective agents [9]. The majority of these reducing and stabilizing materials originate from sources such as bacteria, plants, fungi, and algae [10, 11]. For example, a recent study evaluated the antimicrobial potential of silver and gold NPs biosynthesized using blue-green algae, specifically *Oscillatoria* sp. and *Spirulina platensis* [12]. The NPs were synthesized via 3 distinct approaches—culture-free cells, aqueous extracts, and whole-cell cultivation—with the latter yielding the most bioactive constructs [12]. Whole-cell synthesis yielded NPs with defined morphology and strong antimicrobial activity. Gold NPs exhibit superior efficacy, with MICs as low as 1.1 μg/mL against Candida tropicalis. The study confirms that blue-green algae are sustainable platforms for nanoparticle production, with promising applications in antimicrobial therapy [12]. Raveendran et al. described a technique for synthesizing Ag, Au, and Au-Ag alloy NPs. They used glucose as a reducing agent and starch as a protective agent, resulting in NPs with sizes ranging from 2 to 12 nm [13]. Similarly, Huang et al. found that a tannin extract from Bayberry could act as both a reducing and a protective agent, yielding AuNPs with an average size of 2 nm [14]. AuNPs in the size range of 10-150 nm were synthesized at room temperature using *Nymphaea alba* root extract, as reported by Cudalbeanu et al. [15]. A study by Botteon et al. demonstrates that AuNPs can be synthesized using Brazilian red propolis (BRP) extract, as confirmed by ultraviolet-visible (UV–Vis) spectroscopy [16].

Furthermore, they showed that the size and morphology of the resulting AuNPs were influenced by the specific BRP fractions employed, namely hexane, dichloromethane, and ethyl acetate [16]. Huang et al. used *Heracleum persicum* grass extract as a reducing agent to create AuNPs with an average diameter of approximately 26 nm. They studied its anticancer properties in gastric cancer cells and its potential for electrochemical nitrite sensing [17]. On the other hand, Gharari et al. used *Scutellaria multicaulis* root extract to synthesize 24 nm AuNPs and investigated its anticancer, antibacterial, and antioxidant properties [2]. Gharari et al. synthesized silver NPs with an average size of 60 nm using the stem extract of *S. multicaulis* [18]. This study provides an in-depth examination of the synthesis, characterization, and biological activity assays of AuNPs using 4 different plant extracts: root extracts of *Sanguisorba officinalis* and *S. multicaulis*, and stem and fruit extracts of *H. persicum*.

Materials and Methods

Preparation of extracts

Fresh, healthy, and mature stems of *S. multicaulis* (Sm-S) and *H. persicum* (Hp-S), roots of *S. officinalis* (So-R), and fruits of *H. persicum* (Hp-F) were gathered from their native growing region in northwest Iran. The plant materials were meticulously rinsed with distilled water and left to dry at ambient temperature. The dried components were then pulverized into a fine dust using a grinding device. Following this, 5 g of the powdered specimen was heated in 100 mL of distilled water at 90 ˚C for 30 min. The aqueous extracts were cooled down to room temperature and filtered using Whatman No. 1 filter paper. The resulting aqueous extracts were stored at 4 ˚C for later use in the synthesis of AuNPs [2].

Synthesis of AuNPs

The biosynthesis of AuNPs was conducted using a method described by Gharari et al. with certain modifications [2]. The biological synthesis of AuNPs used Sm-S, Hp-S, So-R, and Hp-F extracts. Gold chloride trihydrate ($HAuCl_4 \cdot 3H_2O$> 99.9%), procured from Sinopharm Chemical Reagent Co., Ltd. (Shanghai, China), was utilized at varying concentrations (0.2, 0.4, 0.6, 0.8, and 1.0 mM). These concentrations were individually added to the aqueous extracts (2%, 3%, 4%, 5%, and 10% v/v). The mixtures were then incubated at 60 ˚C for 30 min. Based on the stability and aggregation properties, the following combinations were selected for subsequent experiments: 0.4 mM $HAuCl_4 \cdot 3H_2O$ with 2% HpS, and 5% each of Hp-F, Sm-S, and So-R extracts. For additional examinations, the AuNPs suspension was centrifuged at 9000 rpm for 30 min. The resulting pellet containing AuNPs was rinsed three times with distilled water to remove contaminants, then preserved at 4 ˚C in a fridge for subsequent use.

Characterization of AuNPs

FE-SEM and EDX spectroscopy analyses of AuNPs

Field-emission scanning electron microscopy (FE-SEM) was used to examine the surface topography, size, and structural properties of biosynthesized AuNPs. The AuNPs were centrifuged at 9000 rpm at room temperature for 30 min. Following centrifugation, the supernatant was discarded, and the AuNPs pellet was dissolved in deionized distilled water. This process was followed by a centrifugation and dispersion process repeated three times. A small drop (0.1 mL) of the nanoparticle aqueous solution was then placed on a glass slide to form a thin film. This film was allowed to dry at room temperature. The cover slip was subsequently prepared for FESEM analysis. The images of AuNPs were captured using a FESEM (ZEISS Sigma 300, Germany) [19]. The energy-dispersive X-ray spectroscopy (EDX) method was employed to examine the elemental composition and chemical properties of AuNPs, using a FESEM-EDX (Carl Zeiss Sigma 300 VP) to acquire the EDX spectrum [20].

Dynamic light-scattering (DLS) and zeta potential (ZP) measurements

To examine the enlargement in the hydrodynamic diameter of AuNPs, which is a result of bio-organics derived from plants adhering to the surface of AuNPs, DLS was conducted using a nanoparticle size analyzer from VASCO, Cordouan Technology, France, in the colloidal mixture. ZP measurements were also conducted using a Zetasizer Nano ZS (Malvern Instruments) in a disposable cell at 25 ˚C, utilizing the Zetasizer software, version 7.01. Both DLS and ZP measurements were employed to assess the stability of the AuNPs. These measurements were initially carried out 2–3 hours post-synthesis of the AuNPs and subsequently once a week for 3 weeks. In between measurements, all AuNP suspensions were stored frozen at −18 ˚C. Before each measurement, the suspension was allowed to thaw and equilibrate at room temperature for 2 hours. Immediately after the measurements, the extracts were refrozen [20].

Fourier transform infrared spectroscopy analysis of AuNPs

Following full bioreduction, the AuNPs underwent a washing step by centrifugation at 10000 rpm for 15 min, after which they were redispersed in distilled water. This procedure was carried out three times. The resulting purified pellet was dried and then subjected to a Fourier transform infrared spectroscopy (FTIR) measurement (FTIR Spectrum 2000, Perkin Elmer, USA) using the potassium bromide (KBr) pellet method in diffused reflection mode at a resolution of 4 cm^{-1}. The Au nanoparticle powder was combined with KBr and then exposed to an IR source that ranged from 400 cm^{-1} to 4000 cm^{-1} [2].

X-ray diffraction (XRD) analysis of AuNPs

XRD analysis was conducted to determine the formation, phase purity, and crystalline nature of the biosynthesized AuNPs. The dried gold NPs were coated onto an XRD grid, and the diffraction patterns were recorded using a Rigaku Ultima IV diffractometer. This procedure was done at room temperature with a Cu-Kα radiation wavelength of λ=0.1540598 nm, within a 2θ range of 20 to 80 θ. The scan rate was set to 0.02°/s, with a time constant of 2 seconds, over 2 hours. The size (D) of the AuNPs was determined using Debye-Scherrer's formula (Equation 1):

1. $D=K\lambda/\beta cos\theta$

In Equation 1, D represents the crystallite size, K is a shape factor (0.9), λ is the X-ray wavelength, β is the full width at half maximum, and θ is the angle according to Bragg's law [18].

Phytochemical content of AuNPs

The TPC of AuNPs and plant extracts was determined spectrophotometrically using the Folin-Ciocalteu reagent. In brief, 20 µL of extract (1 mg/mL) and biosynthesized AuNPs at suitable dilutions (0.1, 0.2, 0.4, 0.8, and 1 mg/mL) were added to a mixture of 100 µL of 10% Folin-Ciocalteu reagent and 80 µL of 7.5% sodium carbonate solution. This mixture was stirred thoroughly at room temperature. Finally, after incubating for 90 minutes in the dark, the samples were measured spectrophotometrically at 765 nm against a deionized water blank. The emergence of a blue color in the mixture indicated the presence of phenolic constituents. To ascertain the actual amount of TPC, a standard curve of Gallic acid was plotted for the standard solutions of Gallic acid (0, 50, 100, 150, and 200 µg/mL). The amount of total phenolic compounds was then expressed as mmol/ L of Gallic acid equivalents (GAE) [2]. The total flavonoid content (TFC) of AuNPs (0.1, 0.2, 0.4, 0.8, and 1 mg/mL) and plant extracts (1 mg/mL) was determined spectrophotometrically using the aluminum chloride colorimetric method. In brief, 20 µL of each sample, 60 µL of ethanol, 10% aluminum chloride (4 µL), 1 M potassium acetate (4 µL), and distilled water (152 µL) were mixed. The mixture was incubated at room temperature (22 °C) for 40 min, and the absorbance was recorded at 415 nm using a UV-visible (Vis) spectrophotometer. The same procedure was performed for the standard solutions of Quercetin (1, 10, 50, 100, 150, and 200 µg/mL), and a calibration curve was plotted. The amount of flavonoid was expressed in terms of quercetin equivalent (mg QE/mL) [2].

In vitro cell viability assay of AuNPs

The toxicity of AuNPs towards MDA-MB -231 (M D Anderson-Metastatic Breast – 231) and HFF2 (Human Fall Flat 2) cells was assessed using the traditional MTT-reduction assay (3-(4,5-dimethyl thiazol-2yl)-2,5-diphenyl tetrazolium bromide) [21]. The MDA-MB-231 cell line, obtained from Iran's National Cell Bank at the Pasteur Institute, was cultivated in Dulbecco's modified eagle's medium (DMEM) supplemented with 10% FBS and 1% antibiotics (streptomycin and penicillin). Cells were placed in a 96-well round-bottom cell culture plate at a concentration of 100000 cells/well and left overnight for adhesion in a CO_2 incubator at 37 ˚C and 95% humidity. Following a 24-h incubation period, the medium was replaced with a mixture of biosynthesized gold NPs at different concentrations (500, 250, 125, 60, and 30 µg/mL), and the process was repeated three times. The root extract of *S. officinalis*, stem extract of *S. multicaulis* and *H. persicum*, and fruit extract of *H. persicum*, all at a density of 1 mg/mL, were utilized as a positive control, with the incubation continuing for another 48 hours. Cells that were untreated and blank samples (cells with dimethyl sulfoxide [DMSO] acting as a solvent) functioned as controls. The cells were subsequently washed with phosphate-buffered saline (PBS) and incubated in a serum-free medium containing 10 µL MTT (5 mg/mL in PBS) for an extra 4 h in darkness at 37 ˚C until the appearance of purple color precipitates. Following this, the supernatant was removed, and the formed formazan crystals were dissolved using 100 µL of DMSO solubilization solution, accompanied by gentle shaking at 37 ˚C for 5 min. The absorbance of each specimen was measured at 570 nm using an ELISA reader (Spectra MAX; Molecular Devices, USA). The cell viability percentage and the AuNPs concentration that resulted in a 50% de-

crease in cell viability (ie, IC_{50} value) were subsequently computed using the Equation 2.

2. *Cytotoxicity percentage=[(control OD−sample OD)/control OD]×100%*

In Equation 2, OD sample represents the average OD value of the experimental samples (AuNPs), and OD control represents the average OD value of the experimental control (untreated).

Cell apoptosis assay

MDA-MB231 cancer and HFF2 normal cells were planted and subsequently treated with Sm-S-AuNPs at a concentration of 200.47 µg/mL; a culture medium-only control was used as a negative control. The cells were then kept at 37 ˚C for 2 days. After this period, flow cytometry analysis was performed using Annexin V-FITC/PI staining. The treated cells were removed from the plates by applying 200 µL of trypsin, a process known as trypsinization. These cells, post-trypsinization, were collected by spinning at 1700 rpm for 4 min at 4 ˚C. The cells underwent two washes with PBS and were then redissolved in a binding buffer to reach a final cell density of 1×10^6 cells/mL [19]. To assess apoptosis and necrosis, an Annexin V-FITC/PI staining kit was used to stain 500 µL of the cell suspension, following the manufacturer's guidelines. The stained cells were subsequently examined by flow cytometry using a system supplied by Becton, Dickinson and Company (BD), located in Sunnyvale, CA, USA.

Statistical analysis

Every experiment was conducted three times, with the outcomes shown as the Mean±SD. The data's significance was statistically evaluated using a one-way analysis of variance (ANOVA), followed by Duncan's new multiple range test. A $P<0.01$ was deemed to have statistical significance.

Results and Discussion

Biosynthesis of AuNPs

AuNPs are typically produced by adding a reducing agent to a solution of $HAuC_4 \cdot 3H_2O$. This procedure diminishes the gold ions and leads to the clustering of the Au atoms into AuNPs. A variety of organic compounds are frequently incorporated to form a protective coating on the AuNPs' surfaces, thereby inhibiting their consolidation into larger particles. This research outlines an eco-friendly method for producing So-R-AuNPs, Sm-S-AuNPs, Hp-S-AuNPs, and Hp-F-AuNPs using environmentally benign substances. We investigated the activity of extracts from four common plants: *S. officinalis* root extract, *S. multicaulis* and *H. persicum* stem extracts, and *H. persicum* fruit extract, as reducing and protecting agents. The resulting AuNPs were thoroughly studied, with their size, shape, spectral characteristics, phytochemical content, antioxidant, and anticancer activity examined.

UV-Vis absorption analysis

The outcomes of reactions between various aqueous extracts (% v/v) and Au (III) concentrations (mM), conducted at 60 ˚C for 30 min, are depicted in Figures 1a, 1b, 1c and 1d. The solution's ruby red hue is attributed to the excitation of surface plasmon resonance (SPR) in the AuNPs. A mixture comprising 0.4 mM $HAuC_4 \cdot 3H_2O$, 2% Hp-S, and 5% each of Hp-F, Sm-S, and So-R extracts resulted in the most stable colloid, exhibiting no aggregation (Figures 1a, 1b, 1c and 1d). The Figure 1 shows the UV-Vis spectra of So-R-AuNPs, Sm-S-AuNPs, Hp-S-AuNPs, and Hp-F-AuNPs, each displaying a strong absorption peak at 531, 541, 546, and 562 nm, respectively. This finding indicates successful biosynthesis, a phenomenon not observed in the absorption spectra of the aqueous extracts of So-R, Sm-S, Hp-S, and Hp-F (Figures 1e, 1f and 1h).

These findings align with those of Gharari et al. who synthesized biogenic gold NPs using *S. multicaulis* root extract [2]. As a result, these synthesized AuNPs were chosen for further characterization and experiments.

Characterizations of AuNPs

FESEM analysis of AuNPs

Particle size distribution and elemental mapping of AuNPs were revealed by FESEM measurement. FESEM images of the AuNPs formed by the four extracts revealed particles of similar shapes and sizes (Figures 2a, 2c, 2e and 2g). Images from FESEM confirmed that the biosynthesized gold particles had a nanoscale. In addition, FESEM images of the produced AuNPs showed that most NPs were spherical. A histogram depicting the distribution of particle sizes was constructed from the dimensions of 100 Au-NPs, as illustrated in Figures 2b, 2d, 2f, and 2h. As per the histogram, the average particle size values of So-R-AuNPs, Sm-S-AuNPs, Hp-S-AuNPs, and Hp-F-AuNPs were 22.61, 22.48, 16.9, and 18.7 nm in diameter, respectively, with a standard devia-

PBR
Pharmaceutical & Biomedical Research

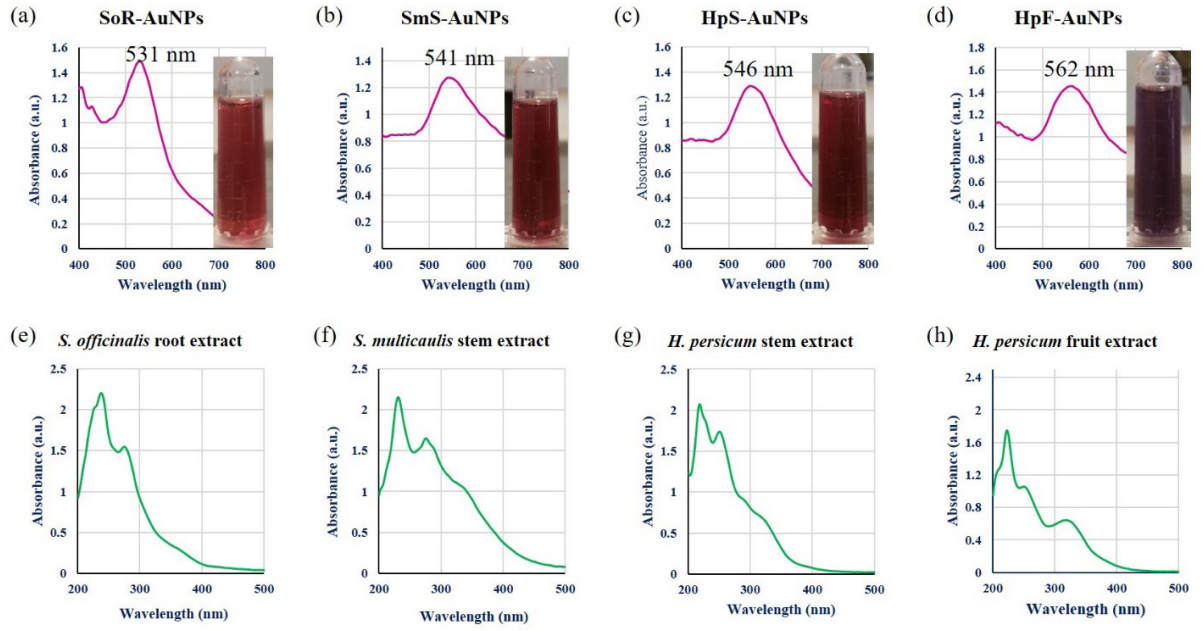

PBR

Figure 1. a-d) AuNPs synthesized following reaction between various aqueous extracts (%v/v) of So-R, Sm-S, Hp-S, and Hp-F, and different concentrations (mM) of Au (III); e-h) The UV-Vis spectrum of the aqueous extracts of So-R, Sm-S, Hp-S, and Hp-F
Abbreviation: Sm-S: Stems of *S. multicaulis*; Hp-S: Stems of *H. persicum*; So-R: Roots of *S. officinalis*; Hp-F: Fruits of *H. persicum*.
Note: The reaction was conducted at 60 ˚C for 30 minutes.

tion of 4.12, 5.02, 4.27, and 4.59 nm. The sizes of So-R-AuNPs, Sm-S-AuNPs, Hp-S-AuNPs, and Hp-F-AuNPs ranged from 16 to 30 nm, 11.7 to 38.3 nm, 6 to 26 nm, and 12 to 28 nm (Figure 2). Spherical AuNPs were reported by other researchers [2]. NPs of such forms can readily traverse the cell membrane. As a result, they can impair targeted cellular organelles and enzymatic systems, leading to cell damage and subsequent induction of apoptosis [22-24].

EDX analysis of AuNPs

The elemental composition of AuNPs was ascertained using EDX. In other words, the strong signal from gold atoms indicates successful synthesis of AuNPs. In Figure 3a, the EDX spectrum of So-R-AuNPs, recorded in the spot-profile mode from one of the densely populated AuNPs area, showed the presence of Au as the major element (70.8%). Other chemical elements, such as C (17.8%), O (5.7%), N (2.8%), Si (2.3%), and Na (0.6%), according to the EDX spectra of Sm-S-AuNPs, are shown in Figure 3b. It was determined that, despite the presence of a gold signal (91.4%) as the principal element, other chemical elements, such as C (6.8%) and O (1.7%), were observed in the EDX spectrum. The EDX plot of Hp-S-AuNPs in Figure 3c approves the chemical composition of gold in terms of atomic percentage (90.5%). Simultaneously, EDX measurement showed the presence of 7.9% of carbon and 1.7% of oxygen in the structure of Hp-S-AuNPs. Furthermore, according to the EDX spectra (Figure 3d), it can be determined that the Hp-F-AuNPs are composed of gold (76.1%), with traces of carbon (13.9%), oxygen (7%), and chlorine (3%). The appearance of a silicon signal in the EDX spectrum of So-R-AuNPs can be related to the thin coating created on the glass substrate used for the EDX. The EDX data verified that the fabricated NPs contained gold in their structure (Figures 3a, 3b, 3c, and 3d) and validated the conversion of gold chloride to gold. The faint signals of C, N, Na, Cl, and O were probably due to X-ray emission from enzymes/carbohydrates/proteins located in the cell wall of the biomass enveloping the NPs [2, 20]. It was reported that similar outcomes were observed in biogenic synthesis using *S. multicaulis* stem and leaf extracts and Cichorium intybus leaf-derived callus extract [18, 19, 22].

DLS analyses of AuNPs

The hydrodynamic diameters of the suspended AuNPs were gauged using the DLS method. This technique uses dynamic light scattering (DLS) to determine the average particle size and the radius distribution of NPs. The result is shown in Figure 4, where the scattering inten-

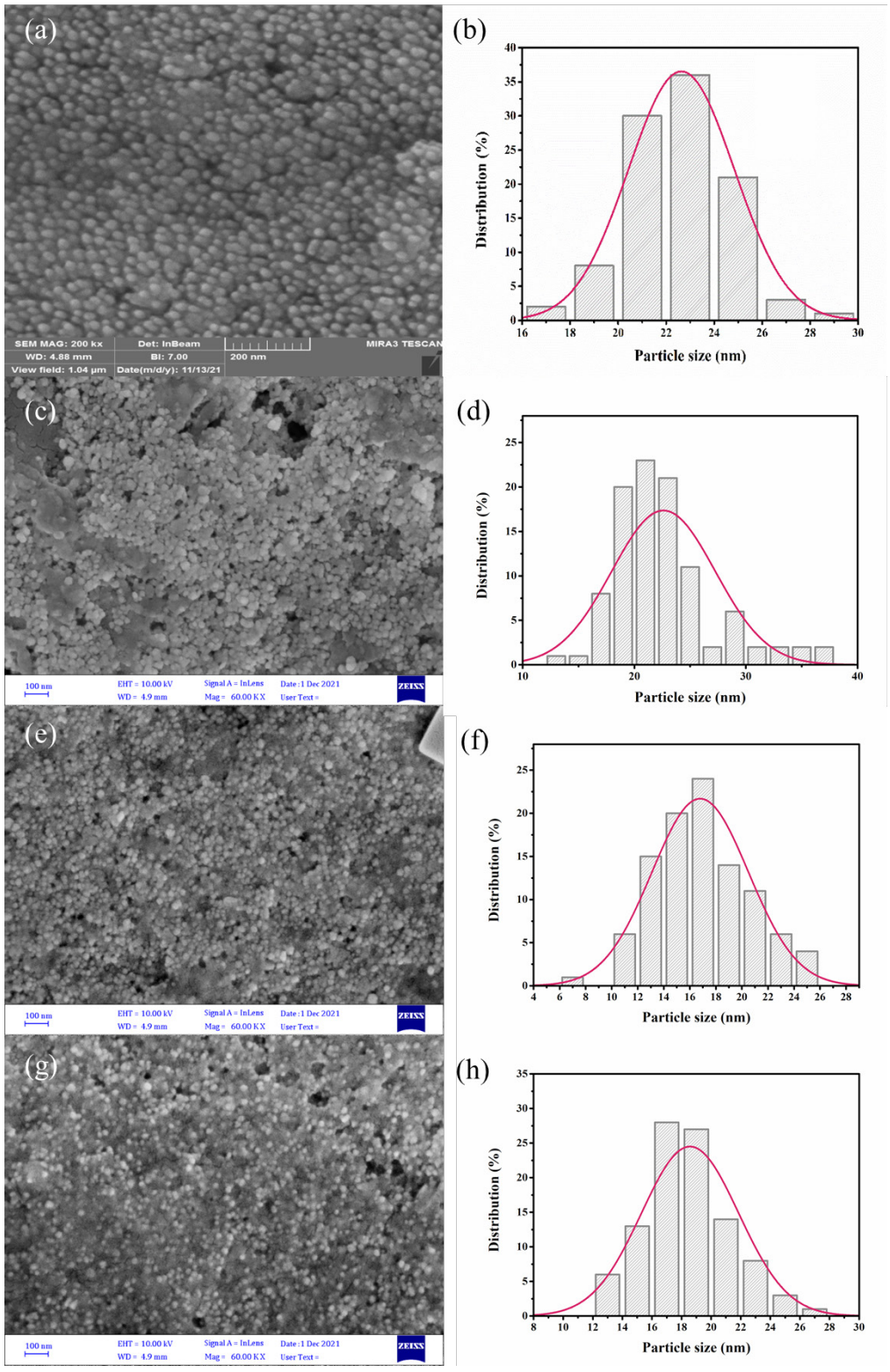

Figure 2. FESEM image and histogram of particle size distribution of a) So-R-AuNPs, b) Sm-S-AuNPs, c) Hp-S-AuNPs, and d) Hp-F-AuNPs

Abbreviation: Sm-S: Stems of *S. multicaulis*; Hp-S: Stems of *H. persicum*; So-R: Roots of *S. officinalis*; Hp-F: Fruits of *H. persicum*.

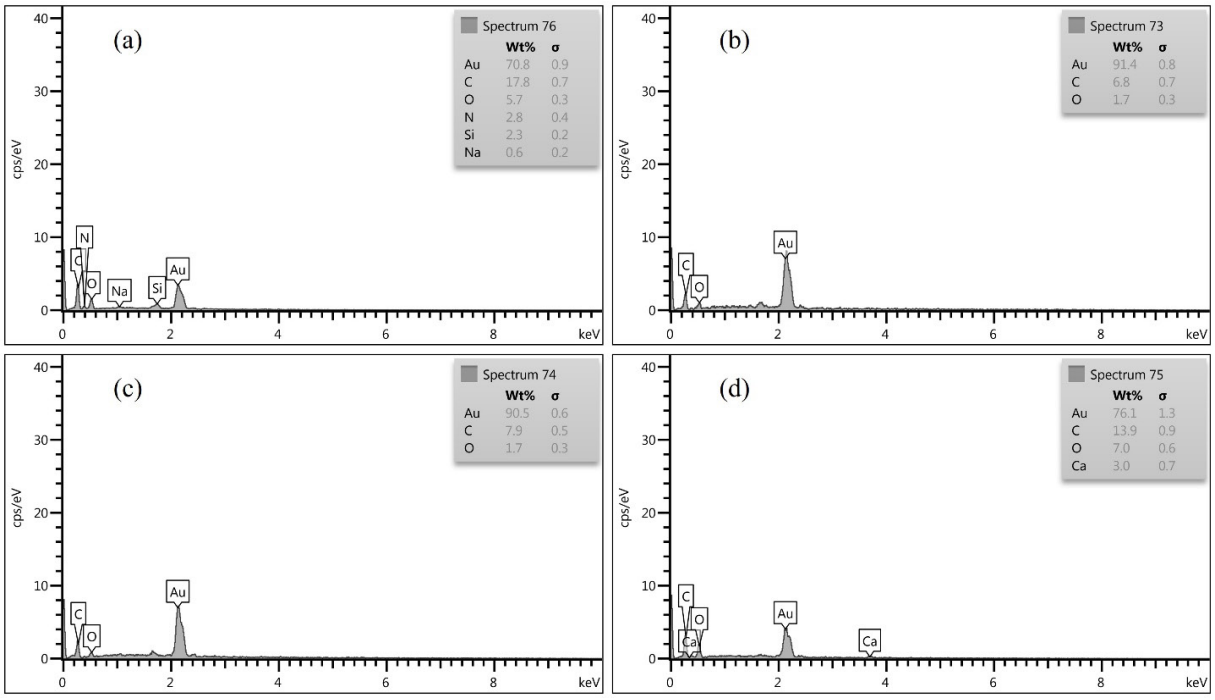

Figure 3. EDX Spectrum of a) So-R-AuNPs, b) Sm-S-AuNPs, c) Hp-S-AuNPs, and d) Hp-F-AuNPs
Abbreviation: Sm-S: Stems of *S. multicaulis*; Hp-S: Stems of *H. persicum*; So-R: Roots of *S. officinalis*; Hp-F: Fruits of *H. persicum*.

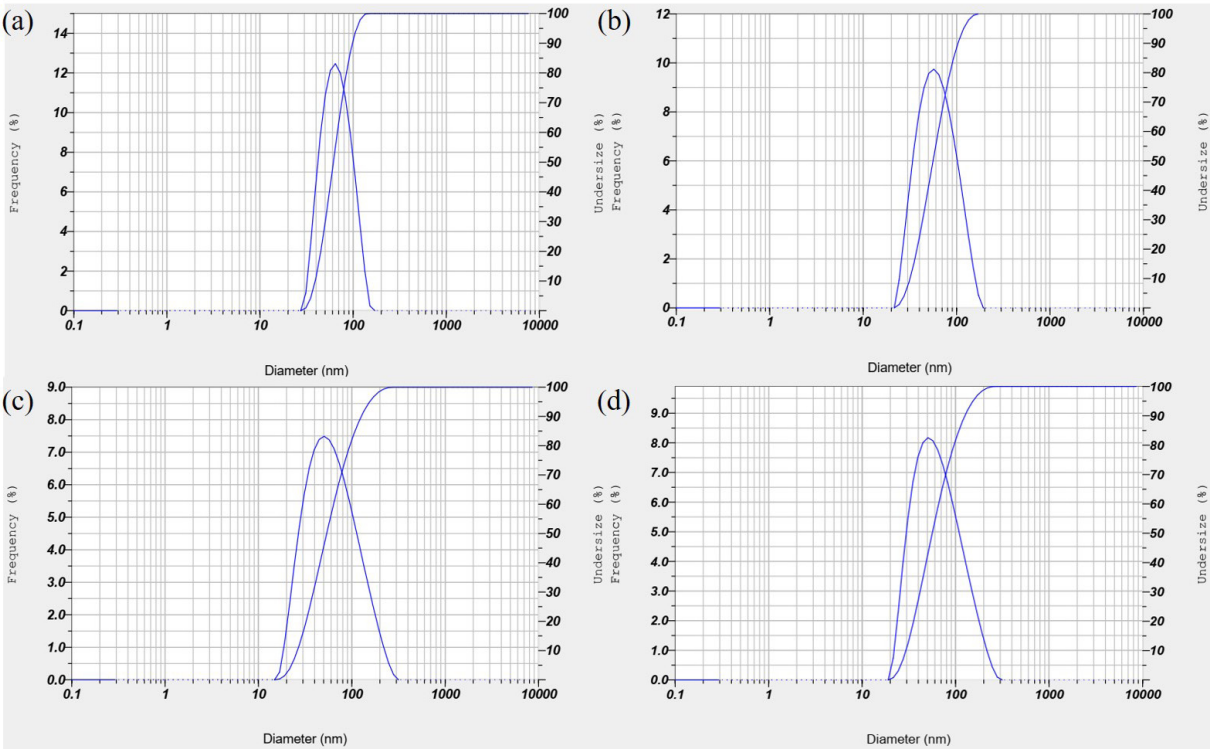

Figure 4. Size distribution analysis of a) So-R-AuNPs, b) Sm-S-AuNPs, c) Hp-S-AuNPs, and d) Hp-F-AuNPs
Abbreviation: Sm-S: Stems of *S. multicaulis*; Hp-S: Stems of *H. persicum*; So-R: Roots of *S. officinalis*; Hp-F: Fruits of *H. persicum*.

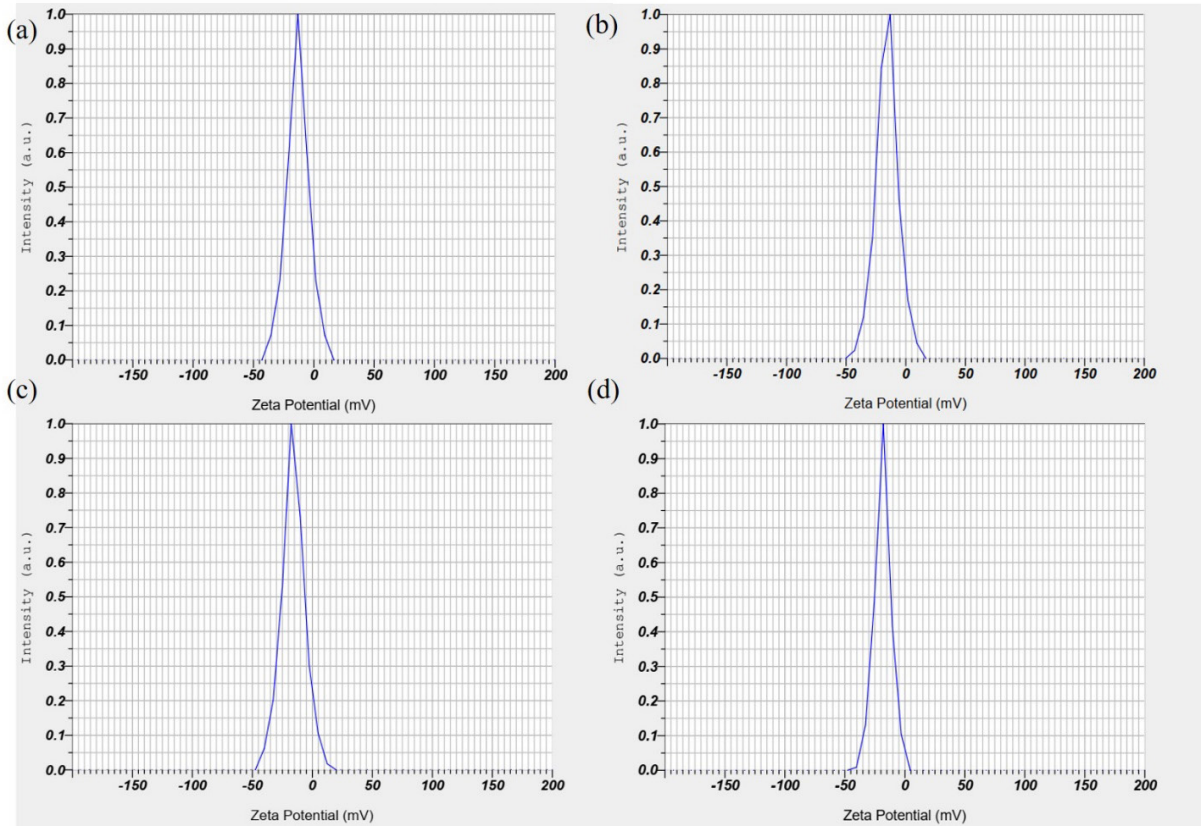

Figure 5. ZP spectra analysis of a) So-R-AuNPs, b) Sm-S-AuNPs, c) Hp-S-AuNPs, and d) Hp-F-AuNPs
Abbreviation: Sm-S: Stems of *S. multicaulis*; Hp-S: Stems of *H. persicum*; So-R: Roots of *S. officinalis*; Hp-F: Fruits of *H. persicum*.

sity is plotted against the logarithm of the NP diameters. The average hydrodynamic size of So-R-AuNPs, Sm-S-AuNPs, Hp-S-AuNPs, and Hp-F-AuNPs was found to be ~43.5 nm, 40.1 nm, 38.3 nm, and 30.5 nm, respectively, confirming that the majority of the particles were under 45 nm (Figures 4a, 4b, 4c and 4d).

The polydispersity index (PDI) is an assessment of the uniformity or diversity of NPs, derived from particle size and denoting the proportion of NPs of varying sizes relative to the overall quantity of NPs. Per the guidelines of the International Standards Organization (ISO), metallic NPs, particularly gold and silver, are deemed monodisperse and potentially less aggregated if their PDI is less than 0.5 or 0.1. Conversely, samples with a PDI>0.7 or =1 are typically considered polydisperse and may be aggregated. In this study, the PDI indices of 0.112, 0.107, 0.131, and 0.117 (<0.3) for So-R-AuNPs, Sm-S-AuNPs, Hp-S-AuNPs, and Hp-F-AuNPs indicated good monodispersity, small size, and homogeneous distribution of AuNPs.

Because it relies on light-scattering intensity, DLS measures the hydrodynamic diameter of NPs in colloidal suspensions, including not only the core particle but also the surrounding solvation shell and any adsorbed biomolecules or stabilizing agents. This issue often leads to an overestimation of particle size, particularly in polydisperse or anisotropic systems, as larger particles scatter light more strongly and disproportionately influence the intensity-weighted distribution. In contrast, FESEM provides direct visualization of the dried NPs, reflecting their actual physical dimensions without hydration or surface-bound layers. XRD, using the Scherrer equation, estimates the average crystallite size from peak broadening, which typically yields smaller values because it reflects only the coherent crystalline domains rather than the entire particle. These methodological differences explain the consistently larger particle sizes observed by DLS compared to FESEM and XRD, as also reported in a previous study on plant-mediated gold nanoparticle synthesis [2]. Accordingly, the size discrepancy in our results is consistent with the literature and underscores the importance of multimodal characterization for accurate nanoparticle profiling [18, 22].

ZP intensity

The ZPs of the AuNPs in all four samples were gauged at 25 ˚C. The AuNPs across all samples displayed negative ZP values ranging from −13 to −18 mV, a range typically indicative of emerging stability for colloids. The ZP distribution for So-R-AuNPs, Sm-S-AuNPs, Hp-S-AuNPs, and Hp-F-AuNPs was determined to be −13.2 mV, −15.7, −16.1, and −18.4, respectively (Figures 5a, 5b, 5c and 5d).

This finding aligns with the average particle diameters (Figure 4). The So-R-AuNPs, created using the root extract of *S. officinalis*, exhibited a lower ZP, suggesting they were less stable and therefore more likely to aggregate and generate larger particles (Figure 5a). On the other hand, the Hp-F-AuNPs, produced using the fruit extract of *H. persicum*, demonstrated the highest ZP, signifying they were more stable and thus less likely to aggregate and create larger particles (Figure 5d). The negative potential value might be due to the encapsulating effect of the biomolecules in the plant extracts being examined. A high negative ZP value indicates a tendency towards electrostatic stability and a significant electrical charge on the AuNPs' surface, resulting in a powerful repulsion among the AuNPs. This repulsion helps prevent aggregation and suggests greater stability of the AuNP colloid [19, 20].

FTIR analysis of AuNPs

FTIR spectra were procured from both the pure extracts and the AuNPs, as depicted in Figure 6. The FTIR spectrum of AuNPs was recorded within the transmittance range of 400 cm^{-1} to 4000 cm^{-1}. The primary objective was to recognize absorption bands that showed significant shifts between the two samples. It was hypothesized that these shifts in peak locations were associated with the adsorption of extract components onto the AuNPs' surfaces. In all 4 cases, the spectra acquired for the two phases under study were remarkably similar (Figure 6). The spectra of the extract and the colloidal solution exhibited a high degree of similarity, suggesting the presence of the same compounds in both samples. However, despite this similarity, some absorption peaks showed significant shifts in position (Figure 6). The FTIR analysis revealed visible bands at 597, 1078, 1102, 1357, 1635, 1722, 2424, 2875, and 2929 cm^{-1} in the FTIR spectrum pattern derived from the So-R (Figure 6a). In the FTIR spectrum of So-R-AuNPs, peaks were observed at 590, 1120, 1342, 1460, 1521, 1542, 1562, 1635, 1741, 2856, 2925, and 3442 cm^{-1}, respectively. Peaks at 572, 1114, 1382, 1521, 1618, 1722, 2856, and 2925 cm^{-1} were identified in the FTIR spectrum of the Sm-S extract (Figure 6b). In the FTIR spectrum of Sm-S-AuNPs, peaks were observed at 595, 1047, 1367, 1458, 1521, 1541, 1560, 1651, 2854, 2923, and 3444 cm^{-1}, respectively. In the spectrum pattern from the Hp-S extract, peaks were detected at 1078, 1271, 1384, 1537, 1618, 1718, and 2931 cm^{-1}, respectively (Figure 6c). In the FTIR spectrum of Hp-S-AuNPs, peaks were observed at 595, 1039, 1460, 1523, 1541, 1562, 1651, 2852, 2925, and 3444 cm^{-1}, respectively (Figure 6c). Peaks at 1028, 1407, 1458, 1616, 1722, 2873, and 2929 cm^{-1}, respectively, were identified in the FTIR spectral pattern derived from the Hp-F extract (Figure 6d). In the spectrum of Hp-F-AuNPs, peaks were observed at 580, 1045, 1361, 1460, 1521, 1541, 1560, 1649, 1747, 2854, 2925, and 3446 cm^{-1}, respectively (Figure 6d). The peaks observed at 580-595 cm^{-1} indicate an O-H out-of-plane (bend) in the polysaccharide moieties produced [25]. The band observed at 1039-1047 cm^{-1} is associated with the C–N stretching vibration of aliphatic amines, alcohols/phenols, or a combination of both [26]. The absorption peak observed at 1342-1367 cm^{-1} corresponds to the -NH stretching of the amide I group of proteins in plant extracts [27]. The peaks at 1458-1460 cm^{-1} can be assigned to hydroxyl groups/phenols or to the -NH bend/amide I [28].

The peak observed in the range of 1521-1523 cm^{-1} is indicative of the bending vibration associated with the primary amine [29]. Meanwhile, the band that appears between 1541-1562 cm^{-1} can be assigned to the nitro N-O groups present in nitroaromatic compounds [30]. The peak within the range of 1635-1651 cm^{-1} can be related to the stretching of the carbonyl (C=O) group in conjugated ketones, or to the vibration of the C=O bond in the amide group [31]. The peak appeared at 1741-1747 cm^{-1} is typically associated with C=O stretching vibrations of carbonyl groups, particularly from esters, aldehydes, or carboxylic acids [32]. Bands in the regions of 2852-2856 cm^{-1} and 2923-2925 cm^{-1} can be attributed to the symmetric and asymmetric C-H/CH_2 stretching vibrations of aromatic compounds, respectively [33]. The FTIR spectra display a significant peak in the 3442-3446 cm^{-1} range, which can be related to the OH-stretching of the alcoholic group [2]. The functional groups mentioned above primarily originate from the So-R, Sm-S, Hp-S, and Hp-F water-soluble components. Therefore, it can be inferred that various water-soluble compounds, such as alkaloids, phenols, proteins, and flavonoids, serve as capping ligands in the synthesis of AuNPs.

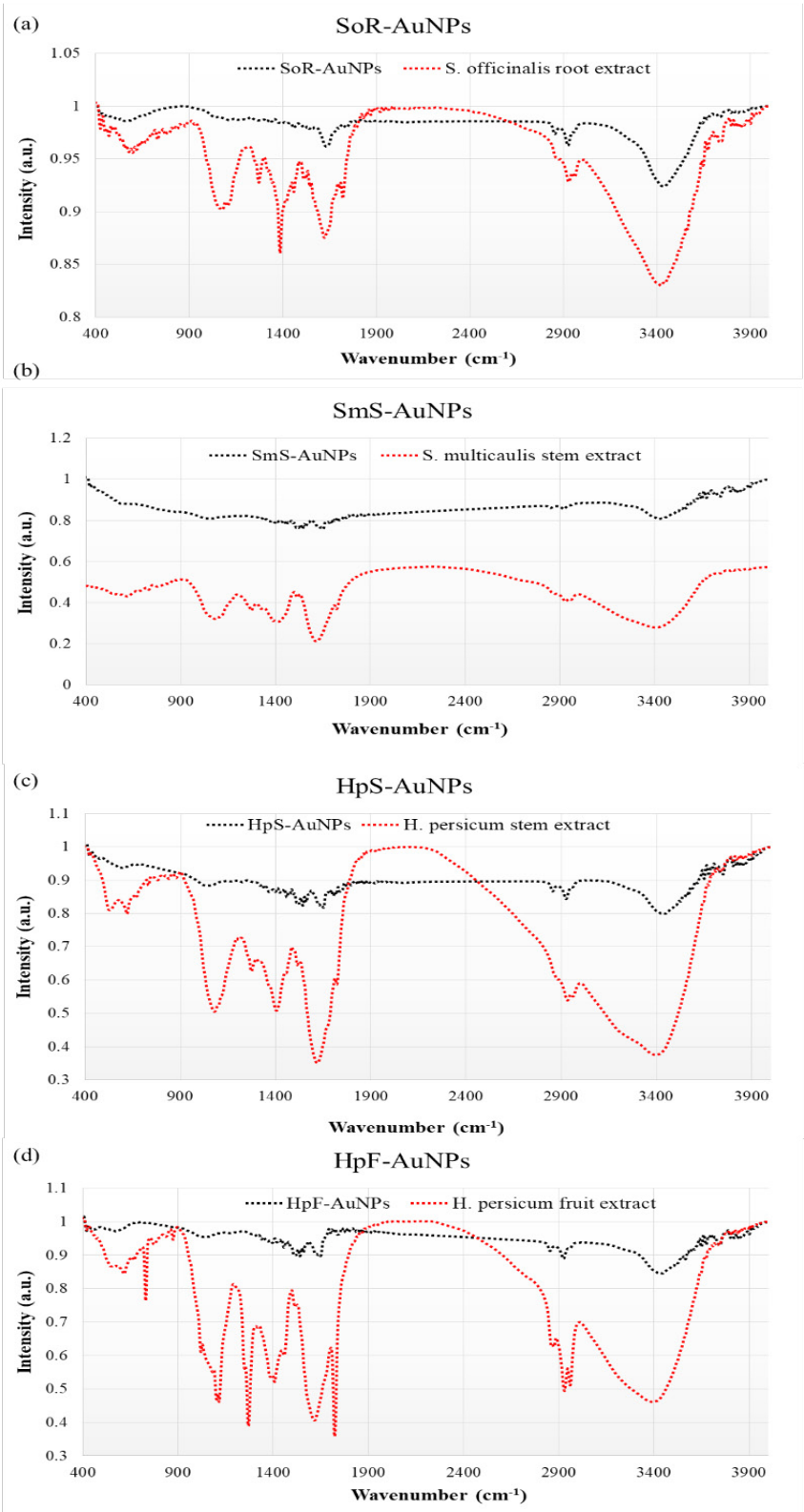

Figure 6. FTIR in the comparative mode showcasing a) So-R-AuNPs, b) Sm-S-AuNPs, c) Hp-S-AuNPs, and d) Hp-F-AuNPs
Abbreviation: Sm-S: Stems of *S. multicaulis*; Hp-S: Stems of *H. persicum*; So-R: Roots of *S. officinalis*; Hp-F: Fruits of *H. persicum*.

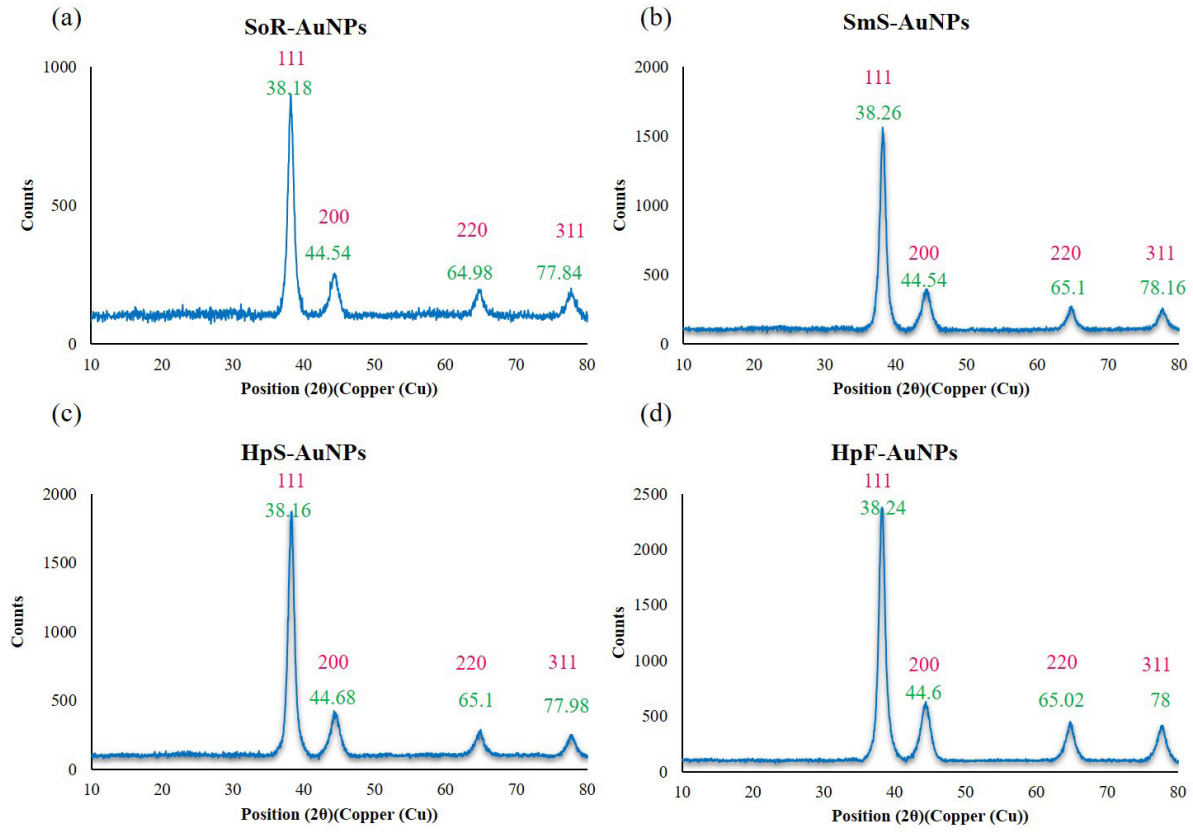

PBR

Figure 7. The XRD spectrum of (a) So-R-AuNPs, (b) Sm-S-AuNPs, (c) Hp-S-AuNPs, and (d) Hp-F-AuNPs

Abbreviation: Sm-S: Stems of *S. multicaulis*; Hp-S: Stems of *H. persicum*; So-R: Roots of *S. officinalis*; Hp-F: Fruits of *H. persicum*.

Table 1. TPC (a) and TFC (b) of So-R-AuNPs, Sm-S-AuNPs, Hp-S-AuNPs, and Hp-F-AuNPs synthesized from So-R, Sm-S, Hp-S, and Hp-F aqueous extract

Sample	Total Phenol Content	TFC
So-R-AuNPs	17.51±0.31	4.72±0.11
So-R	17.49±0.27	4.92±0.09
Sm-S-AuNPs	17.57±0.33	4.5±0.1
Sm-S	17.52±0.38	4.66±0.13
Hp-S-AuNPs	17.52±0.24	4.61±0.15
Hp-S	17.49±0.29	4.69±0.08
Hp-F-AuNPs	17.51±0.18	4.59±0.11
Hp-F	17.52±0.21	4.71±0.12

PBR

Abbreviations: Sm-S: Stems of *S. multicaulis*; Hp-S: Stems of *H. persicum*; So-R: Roots of *S. officinalis*; Hp-F: Fruits of *H. persicum*.

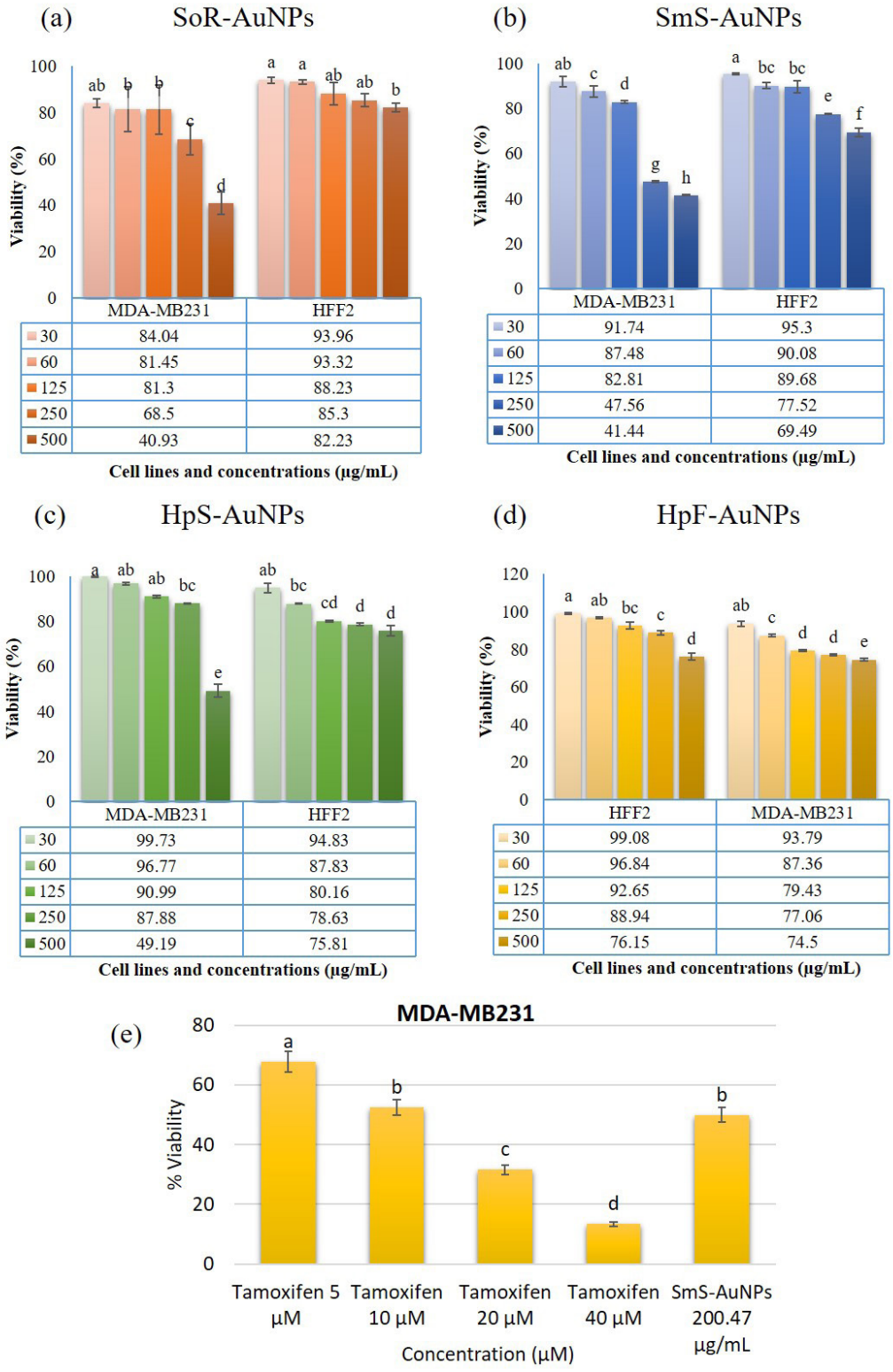

Figure 8. a-d) The impact of aunps on the cytotoxicity of MDA-MB231 and HFF2 Cells; e) The comparison of growth suppression in MDA-MB231 cells by tamoxifen (at doses of 50, 100, 150, and 200 µg/mL) with Sm-S-AuNPs (at a dosage of 200.47 µg/mL) after 48 hours

Abbreviation: Sm-S: Stems of *S. multicaulis*; Hp-S: Stems of *H. persicum*; So-R: Roots of *S. officinalis*; Hp-F: Fruits of *H. persicum*.

Note: The results are presented as Means±SD (n=3).

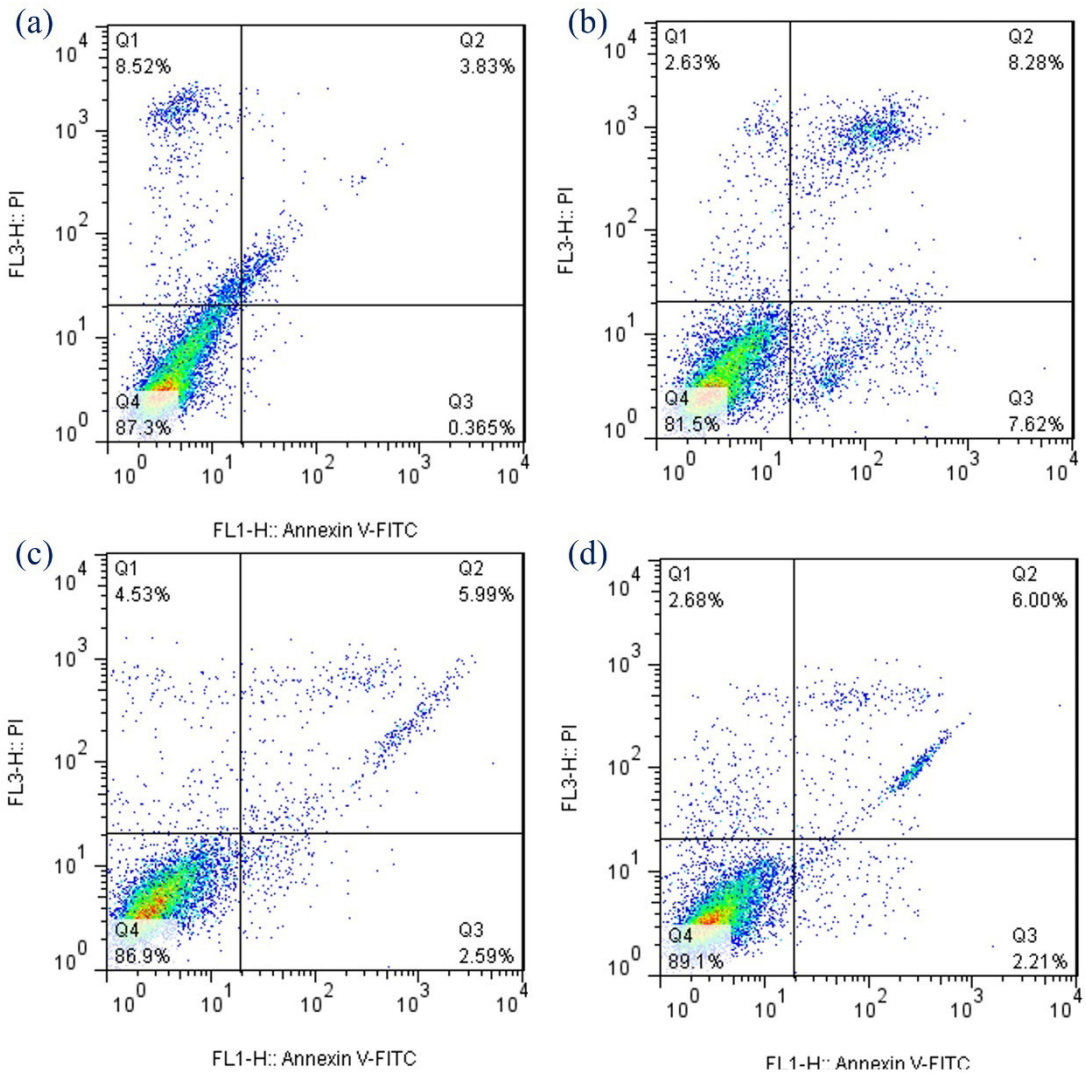

Figure 9. A representative dot plot illustrates the following cell populations: Live cells (annexin-V-FITC-/PI-/lower left quadrant), cells in early apoptosis (annexin-V-FITC+/PI−/lower right quadrant), cells in late apoptosis (annexin-v-fitc+/pi+/upper right quadrant), necrotic cells (annexin-v-fitc-/pi+/upper left quadrant)

a) MDA-MB231 cells without treatment, b) MDA-MB231 cells exposed to 200.47 µg/mL of Sm-S-AuNPs, c) HFF2 cells without treatment, d) HFF2 cells exposed to 200.47 µg/mL of Sm-S-AuNPs

Abbreviations: Sm-S: Stems of *S. multicaulis*; Hp-S: Stems of *H. persicum*; So-R: Roots of *S. officinalis*; Hp-F: Fruits of *H. persicum*.

XRD measurement of AuNPs

Crystallinity of the synthesized AuNPs was confirmed through XRD analysis, and the common XRD patterns are displayed in Figures 7a, 7b, 7c and 7d for So-R-AuNPs, Sm-S-AuNPs, Hp-S-AuNPs, and Hp-F-AuNPs. A characteristic XRD pattern of the Au was identified by Bragg reflections corresponding to (111), (200), (220), and (311) orientation of lattice planes, which can be indexed based on the face-centered cubic structure of AuNPs. The XRD analysis demonstrated four major peaks at 38.32°, 44.54°, 64.98°, and 77.7° for So-R-AuNPs, 38.16°, 44.46°, 65.1°, and 78.16° for Sm-S-AuNPs, 38.18°, 44.54°, 65°, and 78.08° for Hp-S-AuNPs, and 38.24°, 44.54°, 64.88°, and 77.76° for Hp-F-AuNPs. Upon comparing the spectrum with the database, it was determined that the entire spectrum matched JCPDS file No. 00-004-0783, available in X'Pert HighScore. The size of Au-NP particles could be calculated using the Debye-Scherrer formula (Equation 3):

3. $D=\beta cos\theta K\lambda$

where D represents the average crystallite size, β is the line broadening at half the maximum intensity (FWHM),

θ is the Bragg's angle, K is a dimensionless shape factor (0.9), and λ is the X-ray wavelength (0.1540598 nm).

The full-width values at half-maximum (FWHM) of So-R-AuNPs, Sm-S-AuNPs, Hp-S-AuNPs, and Hp-F-AuNPs were 0.018723, 0.019291124, 0.019255345, and 0.019783831, respectively. The FWHM of the most powerful diffraction peak (111) was taken in the Debye-Scherrer's formula to estimate the average crystalline sizes, which were 7.84, 7.61, 7.61, and 7.41 nm for So-R-AuNPs, Sm-S-AuNPs, Hp-S-AuNPs, and Hp-F-AuNPs, respectively, confirming the nano size of the AuNPs [2], which is similar to the average particle size of 22.61, 22.48, 16.9 and 18.7 nm obtained from the FE-SEM image (Figure 2).

Total phenolic and TFCs of AuNPs

Flavonoids and polyphenol compounds, the main phytochemicals in plants, have redox properties and optimal structural features that allow them to function as neutralizers of free radicals. It is proposed that a plant's antioxidant capacity is determined by its overall phenolic and flavonoid content, with a direct relationship observed between these components and antioxidant potential [19]. The TFC and TPC of So-R-AuNPs, Sm-S-AuNPs, Hp-S-AuNPs, and Hp-F-AuNPs synthesized from aqueous So-R, Sm-S, Hp-S, and Hp-F extracts were quantified using the aluminum chloride and Folin-Ciocalteu colorimetric methods, respectively. Analysis of TFC and TPC in So-R, Sm-S, Hp-S, and Hp-F extracts, as well as in So-R-AuNPs, Sm-S-AuNPs, Hp-S-AuNPs, and Hp-F-AuNPs, revealed that TPC was higher in both the extracts and the synthesized AuNPs compared to TFC. However, no statistically significant differences were observed between the TPC and TFC of the plant extracts and those of the synthesized AuNPs (Table 1). The roots and shoots of medicinal plants are abundant in various pharmacologically active substances, such as flavones and phenolic acids, which can play a significant role in the creation of novel cancer treatments [34].

The high concentration of TP compounds in the structure of AuNPs can be due to these metabolites participating in the reduction process during the synthesis of AuNPs. As noted by Marslin et al. (2018), phenolics are the most abundant phytochemicals in the extracts and play an essential role in the bioreduction of metallic ions [35]. Our results align with those of Ahmad et al. (2019), who also reported a higher contribution of phenol and flavonoids in the biosynthesis of AuNPs [36]. Conversely, a minor reduction in the quantity of flavonoid and phenolic compounds in AuNPs relative to the extracts might be due to only a fraction of the phenols and flavonoids extracted from plant extracts being involved in the reduction of Au ions. As such, the noted discrepancy between the two values could result from the use of certain flavonoids and phenols in the creation of AuNPs. Our findings indicate that a larger proportion of flavonoid and phenolic antioxidants from the extracts is involved in the biological production of AuNPs.

Cytotoxicity assay of AuNPs-treated MDA-MB231 cancerous and normal HFF2 cells

Medicinal herbs are key resources for numerous beneficial treatments and potential drug compounds. It is noted that more than half of the anticancer medications currently in use are derived from plants. The synthesis of metallic NPs using medicinal plants is increasingly recognized for its significant contribution to the treatment of various cancer types. In the past few years, metallic NPs created using medicinal plant extracts have been assessed as crucial chemotherapy drugs for various cancers, such as human pancreatic cancer (panc-1), lung adenocarcinoma (A549), breast cancer (MDA-MB231 and MCF-7 cells), and cervical cancer (HeLa) [2, 18-22]. Despite this, there are no scientific reports on the anticancer potential of gold nanostructures biosynthesized using the root extract of *S. officinalis*, the stem extract of *S. multicaulis* and *H. persicum*, and the fruit extract of *H. persicum* against MDA-MB231 breast cancer cells. Hence, the in vitro antiproliferative effects of So-R-AuNPs, Sm-S-AuNPs, Hp-S-AuNPs, and Hp-F-AuNPs, along with the root extract of *S. officinalis*, stem extract of *S. multicaulis* and *H. persicum*, and fruit extract of *H. persicum*, were examined at a concentration of 1 mg/mL. These were tested against MDA-MB231 breast cancer cells and HFF2 cells, which served as a normal cell control. An MTT assay was utilized to perform this screening over 48 hours, with concentrations varying from 30 to 500 µg/mL (Figure 8). The impact of various concentrations of So-R-AuNPs, Sm-S-AuNPs, Hp-S-AuNPs, and Hp-F-AuNPs on the MDA-MB231 cells' proliferation is depicted in Figure 8, parts a-d. A dose-dependent antiproliferative effect on MDA-MB231 cell growth was observed with AuNPs (Figure 8). As the exposure of MDA-MB231 cells to AuNPs increased up to 500 µg/mL, there was a corresponding reduction in cell viability. After 48 h incubation at a concentration of 30 µg/mL, the cells showed viability percentages of 84.4%, 91.74%, 99.73%, and 99.08% for So-R-AuNPs, Sm-S-AuNPs, Hp-S-AuNPs, and Hp-F-AuNPs, respectively (Figure 8). The MDA-MB231 treated cells with 60 µg/mL of So-R-AuNPs, Sm-S-AuNPs, Hp-S-AuNPs, and Hp-F-AuNPs exhibited viability percentages of 81.45%, 87.48%, 96.77%, and 96.84%, respectively (Figure 8).

However, when the cells were exposed to higher concentrations of AuNPs, they revealed the most significant reduction in cell viability at 500 µg/mL of So-R-AuNPs, Sm-S-AuNPs, Hp-S-AuNPs, and Hp-F-AuNPs, with reductions of 40.93%, 41.44%, 49.19%, and 76.15%, respectively. The MTT assay revealed that So-R-AuNPs, Sm-S-AuNPs, Hp-S-AuNPs, and Hp-F-AuNPs had IC50 values of 317.51, 200.47, 491.76, and 664.42 µg/mL, respectively, for MDA-MB231 cells, indicating their strong anticancer properties. Our findings indicated a cell death rate exceeding 58% at a Sm-S-AuNPs concentration of 250 µg/mL (Figure 8b). Notably, AuNPs exhibited no toxicity towards HFF2 normal cells, suggesting these NPs selectively target MDA-MB231 cells (Figure 8). Tamoxifen was used as a positive control at four different concentrations (50, 100, 150, and 200 µg/mL) (Figure 8e). The MTT data indicated that AuNPs can suppress the growth of MDA-MB231 cells, similar to the effect of Tamoxifen (Figure 8e). The selectivity of AuNPs could primarily be attributed to the incorporation of plant-based phytochemicals, such as phenolic acids and flavonoids, into their structure. Smaller AuNPs have the potential to enter cells via endocytosis. In the acidic environment of organelles such as lysosomes and endosomes, AuNPs enhance the generation of oxygen radicals, thereby increasing oxidative stress on cellular components such as DNA and proteins. This condition leads to the cell's self-destruction.

The interaction of AuNPs with the cell membrane or the membranes of internal and external organelles could trigger the release of lipid peroxides, which, in turn, damage the plasma membrane and lead to cell death. The findings of this study indicate that AuNPs could potentially exert antitumor activity on MDA-MB231 cell proliferation in a dose-dependent manner. As a result, additional studies on this plant could help develop novel anticancer drugs to treat breast cancer.

Apoptosis analysis by flow cytometry

Flow cytometry was used to assess the potential of Sm-S-AuNPs to induce apoptosis and necrosis in MDA-MB231 and HFF2 cells. The proportions of live, apoptotic, and necrotic cells were determined using Annexin V-FITC and propidium iodide (PI). MDA-MB231 cells untreated served as the control group. Figure 9a and b display the proportions of apoptotic and necrotic MDA-MB231 cells in cultures that underwent a 48-hour incubation in DMEM medium with 200.47 µg/mL Sm-S-AuNPs. The qualitative examination of apoptotic effects indicated that MDA-MB231 cells were undergoing both apoptosis and necrosis. Following a 48-hour incubation period, the percentage of MDA-MB231 cells undergoing apoptosis increased upon treatment with Sm-S-AuNPs at 200.47 µg/mL, compared with the control cells. The rate of early apoptosis in MDA-MB231 cells exposed to Sm-S-AuNPs was 7.62%, which was higher than the 0.365% observed in the control cells (Figures 9a and 9b). As indicated by the MTT assay in Figure 8b, cell death rates of 52.44% and 58.56% were recorded at concentrations of 250 and 500 µg/mL, respectively, for MDA-MB231 cells. There was a notable increase in the rate of late apoptosis triggered by Sm-S-AuNPs, reaching 8.28%, compared with 3.83% in control cells (Figure 9a, b). Flow cytometric assay revealed that Sm-S-AuNPs amplified the occurrence of early and late apoptotic events in MDA-MB231 cells by 15.9% at a concentration of 200.47 µg/mL. However, both untreated HFF2 cells and those treated with 200.47 µg/mL of Sm-S-AuNPs showed no signs of early or late apoptosis or cell necrosis (Figures 9d and 9e).

The development of novel cancer treatments hinges on creating drugs that are both effective and selectively toxic. In the current study, Sm-S-AuNPs showed no toxic effects on normal HFF2 cells. The disparity in the cytotoxicity of Sm-S-AuNPs towards MDA-MB231 cancerous cells and HFF2 normal cells can be linked to the faster metabolism and quicker division of cancer cells. The properties of NPs and their interaction with biological systems are significantly influenced by their shape. Among the various shapes, spherical AuNPs are frequently reported in scientific studies due to their unique characteristics [2, 24, 37, 38].

NPs with these shapes can traverse the cell membrane with ease. The cell membrane, a selective barrier, regulates the passage of substances. Certain NPs, owing to their minuscule size and other characteristics, can passively permeate the cell membrane, eliminating the need for energy expenditure or specific transport mechanisms within the cell. Upon entry into the cell, NPs can interact with a variety of cellular components, including organelles such as the nucleus and mitochondria, as well as enzymes. These interactions can disrupt normal cellular functions [39]. For instance, NPs can trigger oxidative stress, leading to damage to cellular components [22]. When cells sustain severe damage and are beyond the point of recovery, they are compelled to undergo apoptosis, a form of programmed cell death [40]. This process prevents the spread of damage to other cells. In the context of nanoparticle exposure, if the damage inflicted by NPs is too severe, the cell may be forced into apoptosis [41].

The study demonstrated a simple, eco-friendly, one-step method for synthesizing AuNPs using carboxymethyl chitosan (CMC) as both the reducing agent and stabilizer, where the size and morphology of the AuNPs could be finely controlled by tuning the molecular characteristics of CMC (degree of substitution, substitution positions, molecular weight, and deacetylation) as well as reaction conditions such as temperature, time, pH, and concentrations of NaOH, $HAuCl_4$, and CMC. NaOH addition proved essential for producing uniform spherical NPs. At the same time, mechanistic analysis showed that the hydroxyl and amino groups of CMC reduced Au(III) to Au(0) and its carboxylate groups provided stabilization against aggregation.

The study presented an eco-friendly, microwave-assisted, one-step method for synthesizing spherical gold (Au), silver (Ag), and alloy (Au–Ag) NPs (~10–50 nm) using an aqueous extract from the aerial parts of Rivea hypocrateriformis as both reducing and stabilizing agent, with successful characterization confirmed via UV-Vis (showing SPR peaks at ~550 nm for Au, ~450 nm for Ag, and ~500 nm for the Au–Ag alloy), XRD, FT-IR, FE-SEM/TEM, TGA, and EDAX, and demonstrating enhanced antimicrobial, antioxidant, and anticancer activities—particularly pronounced for the Au–Ag alloy NPs—highlighting their potential as effective, bio-functionalized agents for biomedical applications.

Conclusion

The formation of gold NPs through plant metabolites is a secure process characterized by minimal chemical reactivity, robust stability, and consistent product generation. This method also displays a selective toxic effect on cancer cells, distinguishing it from the chemical method. The use of AuNPs as anticancer agents has recently become a focal point of research in cancer therapy. Metabolites that are biologically active and support eco-friendly biosynthesis of NPs, including flavones, phenolic acids, and terpenoids, are compatible with a wide array of biomedical applications. This research involved the creation of spherical AuNPs using the water-based extract of *S. officinalis* root, stem extracts of *S. multicaulis* and *H. persicum*, and fruit extract of *H. persicum*, which acted as an effective stabilizer and bio-reducer. The successful formation of AuNPs was verified by a range of measurements, including UV-Vis, XRD, FESEM, FTIR, DLS, EDX, and ZP. This research highlights the significant role of plant phytochemicals in the fabrication of AuNPs. The outcome was an enhanced ability to neutralize free radicals and a potential selective cytotoxic effect on the MDA-MB231 breast cancer cell line, as evidenced by suppressed cell proliferation and triggered apoptosis. While the current work provides foundational insights into green-synthesized gold NPs characterization and preliminary bioactivity, we suggest future directions that include in vivo testing to confirm anticancer efficacy and systemic toxicity, molecular pathway elucidation to uncover mechanistic depth, targeted phytochemical analysis to identify key bioactive constituents, and comparative efficacy studies benchmarking plant-synthesized AuNPs against conventional chemotherapeutic agents. These efforts will be essential to advance the translational relevance and therapeutic potential of biogenic nanomaterials.

Ethical Considerations

Compliance with ethical guidelines

There were no ethical considerations to be considered in this research.

Funding

This research was financially supported by Alzahra University, Tehran, Iran (Grant No.: 500-3-589).

Authors' contributions

Conceptualization, methodology, investigation, software, validation, formal analysis, and writing: Zahra Gharar; Investigation and software: Hanie Sadeghinia; Supervision and project administration: Parichehr Hanachi.

Conflict of interest

The authors declared no conflict of interest.

Acknowledgments

The authors thank the Authority of Alzahra University, Tehran, Iran for their project support.

References

[1] Deivayanai VC, Thamarai P, Karishma S, Saravanan A, Yaashikaa PR, Vickram AS, et al. Advances in nanoparticle-mediated cancer therapeutics: Current research and future perspectives. Cancer Pathog Ther. 2024; 3(4):293-308. [DOI:10.1016/j.cpt.2024.11.002] [PMID]

[2] Gharari Z, Khoshnamvand M, Sadeghinia H, Hanachi P. Easy synthesis of gold nanoparticles using Allium ampeloprasum L. aqueous extract: Phytochemical characterization, in vitro antioxidant activities, and cytotoxic effects. Nat Prod Res. 2025; 18:1-5. [DOI:10.1080/14786419.2025.2493182] [PMID]

[3] Kumar P, Chandra P, Verma N, Diksha, Sharma A, Mani M, et al. Gold Nanoparticles: An emerging novel technology for targeted delivery system for site-specific diseases. Curr Drug ther. 2025; 20:345-61. [Link]

[4] Patil T, Gambhir R, Vibhute A, Tiwari AP. Gold nanoparticles: Synthesis methods, functionalization and biological applications. J Clust Sci. 2023; 34(2):705-25. [Link]

[5] Madkour LH. Applications of gold nanoparticles in medicine and therapy. Pharm Pharmacol Int J. 2018; 6(3):157-74. [Link]

[6] Mishra, S, Sundaram, B. Fate, transport, and toxicity of nanoparticles: An emerging pollutant on biotic factors. Process Saf Environ Prot. 2023; 174:595-607. [Link]

[7] Dang Y, Guan J. Nanoparticle-based drug delivery systems for cancer therapy. Smart Mater Med. 2020; 1:10-19. [DOI:10.10.1016/j.smaim.2020.04.001] [PMID]

[8] Adeyemi OS, Otuechere CA, Adewuyi A, Adeyanju AA, Awakan OJ, Otohinoyi DA. Gold nanoparticles in delivery applications. In: Mozafari M, editor. Nanoengineered Biomaterials for Advanced Drug Delivery. Amsterdam: Elsevier; 2020. [Link]

[9] Hano C, Abbasi BH. Plant-Based Green Synthesis of Nanoparticles: Production, Characterization and Applications. Biomolecules. 2022; 12(1):31. [DOI:10.3390/biom12010031] [PMID]

[10] Husen A, Rahman QI, Iqbal M, Yassin MO, Bachheti RK. Plant-mediated fabrication of gold nanoparticles and their applications. In: Husen A, Iqbal M, editors. Nanomaterials and Plant Potential. Cham: Springer; 2019. [Link]

[11] Khan T, Ullah N, Khan MA, Mashwani ZU, Nadhman A. Plant-based gold nanoparticles; a comprehensive review of the decade-long research on synthesis, mechanistic aspects and diverse applications. Adv Colloid Interface Sci. 2019; 272:102017. [DOI:10.1016/j.cis.2019.102017] [PMID]

[12] El-Sheekh MM, Hassan LHS, Morsi HH. Evaluation of antimicrobial activities of blue-green algae-mediated silver and gold nanoparticles. Rend Lincei Sci Fis Nat. 2021; 32(4):747-59. [DOI:10.1007/s12210-021-01016-x]

[13] Godipurge SS, Yallappa S, Biradar NJ, Biradar JS, Dhananjaya BL, Hegde G, et al. A facile and green strategy for the synthesis of Au, Ag and Au-Ag alloy nanoparticles using aerial parts of R. hypocrateriformis extract and their biological evaluation. Enzyme Microb Technol. 2016; 95:174-84. [DOI:10.1016/j.enzmictec.2016.08.006] [PMID]

[14] Huang X, Wu H, Liao X, Shi B. One-step, size-controlled synthesis of gold nanoparticles at room temperature using plant tannin. Green Chem. 2010; 12(3):395-9. [Link]

[15] Cudalbeanu M, Peitinho D, Silva F, Marques R, Pinheiro T, Ferreira AC, et al. Sono-biosynthesis and characterization of AuNPs from Danube Delta Nymphaea alba root extracts and their biological properties. Nanomater. 2021; 11(6):1562. [DOI:10.3390/nano11061562] [PMID]

[16] Botteon CEA, Silva LB, Ccana-Ccapatinta GV, Silva TS, Ambrosio SR, Veneziani RCS, et al. Biosynthesis and characterization of gold nanoparticles using Brazilian red propolis and evaluation of its antimicrobial and anticancer activities. Sci. Rep. 2021; 11(1):1974. [DOI:10.1038/s41598-021-81281-w] [PMID]

[17] Huang Y, Zhang Y, Zhang Y, Liu W, Fang Y, Motlagh M. Novel biogenic preparation of gold nanoparticles decorated on sepiolite clay and evaluation of anticancer effect on gastric cancer cell and electrochemical sensing of nitrite. Environ. Res 2023; 238(Pt 2):117260. [DOI:10.1016/j.envres.2023.117260] [PMID]

[18] Gharari Z, Hanachi P, Walker TR. Green synthesized Ag-nanoparticles using Scutellaria multicaulis stem extract and their selective cytotoxicity against breast cancer. Anal Biochem. 2022; 653:114786. [DOI:10.1016/j.ab.2022.114786] [PMID]

[19] Gharari Z, Hanachi P, Sadeghinia H, Walker TR. Eco-Friendly Green Synthesis and Characterization of Silver Nanoparticles by Scutellaria multicaulis Leaf Extract and Its Biological Activities. Pharmaceuticals. 2023; 16(7):992. [DOI:10.3390/ph16070992] [PMID]

[20] Hanachi P, Gharari Z, Sadeghinia H, Walker TR. Synthesis of bioactive silver nanoparticles with eco-friendly processes using heracleum persicum stem extract and evaluation of their antioxidant, antibacterial, anticancer and apoptotic potential. J Mol Struct. 2022; 1265:133325. [Link]

[21] Charghadchi M, Gharari Z, Sadighian S, Yazdinezhad A, Sharafi A. Green Synthesized Silver Nanostructure Using Rhus coriaria Fruit Extract Inhibits the Growth of Malignant MCF-7 Cell Line. Braz Arch Biol Technol. 2021; 64:e21210069. [DOI:10.1590/1678-4324-2021210069]

[22] Gharari Z, Hanachi P, Sadeghinia H, Walker TR. Cichorium intybus bio-callus synthesized silver nanoparticles: A promising antioxidant, antibacterial and anticancer compound. Int J Pharm. 2022; 625:122062. [DOI:10.1016/j.ijpharm.2022.122062] [PMID]

[23] Keskin C, Atalar MN, Firat Baran M, Baran A. Environmentally friendly rapid synthesis of gold nanoparticles from Artemisia absinthium plant extract and application of antimicrobial activities. J Inst Sci Technol. 2021; 11(1):365-75. [DOI:10.21597/jist.779169]

[24] Keskin C, Baran A, Baran MF, Hatipoğlu A, Adican MT, Atalar MN, et al. Green synthesis, characterization of gold nanomaterials using Gundelia tournefortii leaf extract, and determination of their nanomedicinal (antibacterial, antifungal, and cytotoxic) potential. J Nanomater. 2022; 2022(1):7211066. [Link]

[25] Fouda A, Awad MA, Al-Faifi ZE, Gad ME, Al-Khalaf AA, Yahya R, et al. Aspergillus flavus-mediated green synthesis of silver nanoparticles and evaluation of their antibacterial, anti-candida, acaricides, and photocatalytic activities. Catalysts. 2022; 12(5):462. [Link]

[26] TYAl-Abdullah Z, AL-SHAWI AA, Aboud MN, Al Abdul Aziz B, Al-Furaiji HQM, Luaibi IN. Synthesis and analytical characterization of gold nanoparticles using microwave-assisted extraction system and study their application in degradation. J Nanostruct. 2020; 10(4):682-90. [Link]

[27] Kanchi S, Kumar G, Lo AY, Tseng CM, Chen SK, Lin CY, et al. Exploitation of de-oiled jatropha waste for gold nanoparticles synthesis: A green approach. Arab J Chem. 2018; 11(2):247-55. [Link]

[28] Muddapur UM, Alshehri S, Ghoneim MM, Mahnashi MH, Alshahrani MA, Khan AA, et al. Plant-based synthesis of gold nanoparticles and theranostic applications: A review. Molecules. 2022; 27(4):1391. [DOI:10.3390/molecules27041391] [PMID]

[29] Asariha M, Kiaie SH, Izadi S, Pirhayati FH, Fouladi M, Gholamhosseinpour M. Extended-release of doxorubicin through green surface modification of gold nanoparticles: In vitro and in ovo assessment. BMC Chem. 2022; 16(1):110. [DOI:10.1186/s13065-022-00895-x] [PMID]

[30] Vinay S, Chandrasekhar N, Chandrappa C. Eco-friendly approach for the green synthesis of silver nanoparticles using flower extracts of Sphagneticola trilobata and study of antibacterial activity. Int J Pharm Biol Sci. 2017; 7:145-52. [Link]

[31] Muniyappan N, Pandeeswaran M, Amalraj A. Green synthesis of gold nanoparticles using Curcuma pseudomontana isolated curcumin: Its characterization, antimicrobial, antioxidant and anti-inflammatory activities. Environ Toxicol-Chem. 2021; 3:117-24. [Link]

[32] Arif H, Qayyum S, Akhtar W, Fatima I, Kayani WK, Rahman KU, et al. Synthesis and characterization of zinc oxide nanoparticles at different pH values from Clinopodium vulgare L. and their assessment as an antimicrobial agent and biomedical application. Micromachines. 2023; 14(7):1285. [DOI:10.3390/mi14071285] [PMID]

[33] Kumar B, Smita K, Debut A, Cumbal L. Utilization of Persea americana (Avocado) oil for the synthesis of gold nanoparticles in sunlight and evaluation of antioxidant and photocatalytic activities. Environ Nanotechnol Monit Manag. 2018; 10:231-37. [Link]

[34] Tungmunnithum D, Thongboonyou A, Pholboon A, Yangsabai A. Flavonoids and other phenolic compounds from medicinal plants for pharmaceutical and medical aspects: An overview. Medicines 2018; 5(3):93. [DOI:10.3390/medicines5030093] [PMID]

[35] Marslin G, Siram K, Maqbool Q, Selvakesavan RK, Kruszka D, Kachlicki P, et al. Secondary metabolites in the green synthesis of metallic nanoparticles. Materials. 2018; 11(6):940. [DOI:10.3390/ma11060940] [PMID]

[36] Ahmad T, Bustam MA, Irfan M, Moniruzzaman M, Asghar HMA, Bhattacharjee S. Mechanistic investigation of phytochemicals involved in green synthesis of gold nanoparticles using aqueous Elaeis guineensis leaves extract: Role of phenolic compounds and flavonoids. Biotechnol Appl Biochem. 2019; 66(4):698-708. [DOI:10.1002/bab.1787] [PMID]

[37] Hasan MR, Sharma P, Pilloton R, Khanuja M, Narang J. Colorimetric biosensor for the naked-eye detection of ovarian cancer biomarker PDGF using citrate modified gold nanoparticles. Biosens Bioelectron. 2022; 11:100142. [Link]

[38] Hamelian M, Hemmati S, Varmira K, Veisi H. Green synthesis, antibacterial, antioxidant and cytotoxic effect of gold nanoparticles using Pistacia Atlantica extract. J Taiwan Inst Chem Eng. 2018; 93:21-30. [DOI:10.1016/j.jtice.2018.07.018]

[39] Kang Me, Weng Y, Liu Y, Wang H, Ye L, Gu Y, Bai X. A Review on the Toxicity Mechanisms and Potential Risks of Engineered Nanoparticles to Plants. Rev Environ Contam Toxicol. 2023; 261:5. [Link]

[40] Liu N, Tang M. Toxic effects and involved molecular pathways of nanoparticles on cells and subcellular organelles. J Appl Toxicol. 2020; 40(1):16-36. [DOI:10.1002/jat.3817] [PMID]

[41] Kumar R, Kumar A, Bhardwaj S, Sikarwar M, Sriwastaw S, Sharma G, Gupta M. Nanotoxicity unveiled: Evaluating exposure risks and assessing the impact of nanoparticles on human health. J Trace Elements Miner. 2025; 13:100252. [DOI:10.1016/j.jtemin.2025.100252]

This Page Intentionally Left Blank